THE JOURNAL OF PHYSICAL CHEMISTRY A

Article

pubs.acs.org/JPCA

Chain-Length and Temperature Dependence of Self-Assembled Monolayers of Alkylthiolates on Au(111) and Ag(111) Surfaces

Y. Wang,*[,†,‡] J. G. Solano Canchaya,[§] W. Dong,[∥] M. Alcamí,[†,‡] H. F. Busnengo,[§] and F. Martín[†,‡]

[†]Departamento de Química Módulo 13, Universidad Autónoma de Madrid, 28049 Madrid, Spain

[‡]Instituto Madrileño de Estudios Avanzados en Nanociencia (IMDEA-Nanociencia), Cantoblanco, 28049 Madrid, Spain

[§]Laboratorio de Colisiones Atómicas, Facultad de Ciencias Exactas Ingeniería y Agrimensura, Universidad Nacional de Rosario (UNR) and Instituto de Física de Rosario, Consejo Nacional de Investigaciones Científicas y Técnicas (CONICET), Av. Pellegrini 250, 2000 Rosario, Argentina

[∥]Laboratoire de Chimie, UMR 5182 CNRS, Ecole Normale Supérieure de Lyon, 46 Allée d'Italie, F-69364 Lyon Cedex 07, France

Supporting Information

ABSTRACT: We present a molecular dynamics (MD) study on the structure of self-assembled monolayers (SAMs) of alkylthiolates on various metal surfaces, with especial attention to Au(111) and Ag(111). Variations in the structure of these SAMs as a function of temperature and alkyl-chain length are systematically investigated. The MD simulations are performed by using a recently developed force field based on second-order Møller−Plesset perturbation theory calculations. Good agreement between the present results and the existing experimental data is found on Au(111). On Ag(111) the comparison between theory and experiment is also satisfactory for alkylthiolates with no more than 14 carbon atoms. The dependences of the average tilt angle of SAMs on temperature and chain length are easily understood by means of a simple single-chain model.

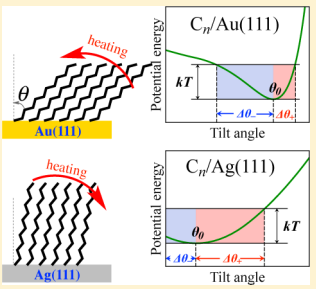

1. INTRODUCTION

During the last decades, self-assembled monolayers (SAMs)[1] have attracted considerable attention in many fields owing to their potential in a variety of technological applications, such as protection of surfaces from corrosion, lubrication, wetting, lithography, molecular recognition, optical and electronic devices, and biosensors.[1−3] In particular, as a prototypical model for SAMs, self-assembled nonbranched alkylthiolates $S(CH_2)_{n-1}CH_3$ (hereafter called C_n) on metal surfaces have been the focus of numerous experimental and theoretical studies, owing to their convenience of preparation, relatively high stability, high structural ordering, good adhesion to the surface, and easiness of functionalization.[1−6]

From the fundamental point of view, SAMs of C_n chemisorbed on Au(111) surfaces have been the object of the most extensive investigations over the last three decades.[7] It is well-known that the saturation coverage is 1/3 monolayer (ML), which is the ratio of the number of molecules to the number of metal atoms of the outermost layer from the ideal unreconstructed surface. Earlier scanning probe microscopy[8] and low-energy electron diffraction (LEED)[9] experiments established that such a densely packed and well-ordered SAM forms a hexagonal arrangement with the nearest neighbor (NN) S−S distance a = 4.97 Å. This structure can be ideally represented by a so-called $(\sqrt{3} \times \sqrt{3})R30°$ unit cell commensurate with the gold lattice (see Figure 1a). Later on, further experiments by means of low-energy helium[10−12] or electron[13] diffraction, grazing incidence X-ray diffraction (GIXD),[14] atomic force microscopy (AFM)[15] as well as scanning tunneling microscopy (STM)[16−19] found an alternative phase of C_n SAM on Au(111) characterized by the so-called c(4 × 2) superlattice of the $(\sqrt{3} \times \sqrt{3})R30°$ unit cell.

Aside from the two-dimensional lattice periodicity, one of the most important structural characteristics of C_n SAMs on Au(111) is the orientation of the molecular chains.[5] It has been generally accepted that on Au(111) surface the C_n backbones are not standing upright on the substrate but significantly tilted away from the surface normal by a certain angle θ (called "tilt angle"; see Figure 1b). The tilt angle can be measured by various experimental techniques, such as GIXD,[14,20,21] reflection absorption infrared (RAIR) spectroscopy,[22−24] near edge X-ray absorption fine structure spectroscopy (NEXAFS),[25,26] surface plasmon spectroscopy[27] and STM imaging.[28] Although the estimated average tilt angle can vary with different experimental methods and conditions, the value typically falls in the range 30−40°, not much dependent on the chain length n.

The ordering of C_n SAMs on Ag(111) at full coverage is also a hexagonal packing[29] but more complicated than on Au(111), although both metals are isoelectronic and have similar lattice parameters in bulk. As revealed by LEED and sum frequency generation (SFG) spectroscopy,[30−32] the structure of C_1 SAM on Ag(111) can be described using a $(\sqrt{7} \times \sqrt{7})R10.9°$ unit cell with an S−S spacing a = 4.41 Å, indicating a denser packing than on Au(111) (a = 4.97 Å). The difference in the SAM

Received: December 16, 2013
Revised: May 21, 2014

   dx.doi.org/10.1021/jp412285v | J. Phys. Chem. A XXXX, XXX, XXX−XXX

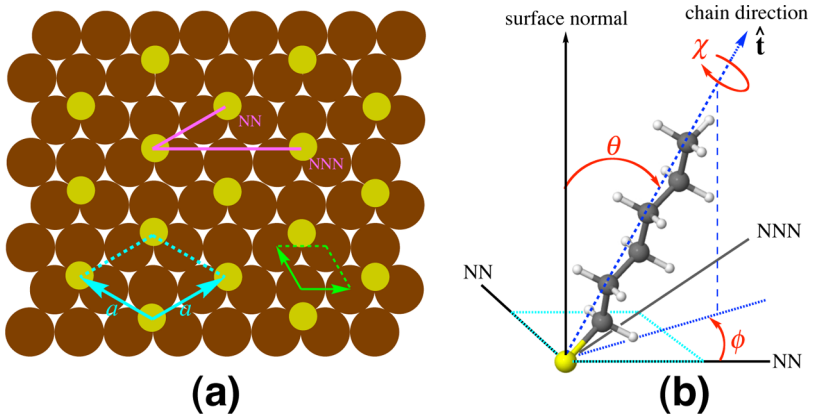

Figure 1. (a) $(\sqrt{3} \times \sqrt{3})$R30° structure of alkylthiolate SAM on (111) surface. Yellow and brown circles represent sulfur headgroups and metal atoms, respectively. The unit cell of the (111) surface and of the SAM is indicated by green and cyan lines, respectively. The red lines point out the nearest neighbor (NN) and the next nearest neighbor (NNN) directions. (b) The definition of three orientational angles, θ, ϕ, and χ, and the vector of the chain direction $\hat{\mathbf{t}}$. Yellow, gray, and white balls represent sulfur, carbon, and hydrogen atoms, respectively. The unit cell of the SAM is also depicted with dotted cyan lines.

structures of C_n between Au(111) and Ag(111) still demands a convincing explanation, for which some theoretical efforts have been made.[33]

From the theoretical side, a large number of simulations[34−58] have been carried out for these systems, especially for C_n SAMs on Au(111) surfaces. There are two aspects that theory tries to elucidate.[59] The first one is the interaction between the molecules and the metal substrate, which determines adsorption sites and geometries of the adsorbate as well as possible reconstructions of the surface. To describe satisfactorily such a molecule−substrate interaction, density functional theory (DFT) computations are usually performed. Due to their expensive computational cost, however, normally only static calculations are carried out to search for minimum energies and structures and the systems are generally limited to short-chain molecules (mostly methylthiol) on unreconstructed surfaces (mostly Au(111)). The other aspect is the intermolecular chain−chain interaction among the molecules, which determines, at least to a considerable extent, the arrangement of the SAM, especially for long-chain molecules. Unfortunately, standard DFT calculations capable of coping with molecule−surface interaction cannot treat properly the vdW interaction between alkyl chains, which instead requires time-consuming high-level quantum chemical computations[60,61] or the use of (usually empirical) corrective terms to standard DFT.[62,63] For molecular dynamics (MD) and Monte Carlo (MC) simulations,[46−58] empirical force fields (FFs) have been employed to describe the chain−chain interaction among alkylthiolates. Both united-atom (UA)[46] and explicit-atom (EA)[43,64] FFs have been developed and compared[37] for SAMs of alkylthiolates on Au(111) surface. The former FF model treats $-CH_2$ and $-CH_3$ groups as single interaction sites, while in the latter model all the atoms are explicitly represented. These FFs can provide a reasonably accurate description of the dynamics of projectile/SAM collisions when used in chemical dynamics simulations. Recently, we have developed an alternative EA FF to describe the intermolecular interaction of alkanethiols, based on second-order Møller−Plesset perturbation theory (MP2) computations.[60] Although the previous FFs also give accurate SAM structures, the tests of these structures in previous studies are not as extensive as in our work. As an alternative option to other FFs, it has been shown[33,60] that our FF is also able to predict the lowest-energy molecular orientations of C_n SAMs on Au(111) and Ag(111) in agreement with experiments. For this reason, the choice of such force field seems appropriate to investigate temperature effects which are more pronounced for shorter chains, where explicit-atom effects are expected to play a role.

In this paper, we present a systematic study of C_n (n = 3−20) SAMs on various surfaces with emphasis on Au(111) and Ag(111) at different temperatures using atomistic MD simulations with the above-mentioned new FF. We will focus on hexagonally packed C_n SAMs at saturation coverage. In particular, we are interested in how the average tilt angle of the SAMs on metal surfaces depends on the molecular chain length and the temperature. This interest is not only of fundamental importance but also has practical potential such as the electronic transport properties of SAM-based devices. A recent experiment[65] on SAMs of C_{12}, C_{16}, and C_{18} on Au(111) surface has clearly revealed that the tilting of the molecular chains enhances significantly the junction conductance as well as the surface work function, and such enhancement strongly depends on the chain length. As observed in a more recent experiment,[66] the increase of temperature gradually reduces the tilt angle of the SAMs of C_n (n = 12−18) that are chemisorbed on silicon surface, which consequently decreases the electronic current through the SAMs.

The rest of the paper is organized as follows. Section 2 details the methodology and setup of the simulations. Results are presented in section 3 and discussed in section 4, followed by the last section where conclusions are drawn.

2. COMPUTATIONAL DETAILS

2.1. Model Systems. In this study, we have systematically examined the hexagonally arranged alkylthiolate SAMs with various chain lengths (from C_3 to C_{20}) on Au(111) and Ag(111) surfaces at different temperatures (T = 300, 200, 100, 50, and 10 K). Apart from the NN S−S spacings of 5.00 Å (Au(111)) and 4.42 Å (Ag(111)), we have also investigated the SAMs with other NN distances, such as 4.80, 4.85, and 4.90 Å, in order to explore the dependence on the NN spacing a.

All the alkylthiolate molecules take an all-trans zigzag conformation, since it has been shown that gauche defects are generally less than 5% in C_n on Au(111), Ag(111), and

dx.doi.org/10.1021/jp412285v | J. Phys. Chem. A XXXX, XXX, XXX−XXX

Pt(111) at 300 K.[54] The orientation of an alkylthiolate molecule is represented by three angles: tilt angle θ, tilt direction ϕ and twist angle χ. The bakcbone direction can be conveniently represented by the line connecting the sulfur atom and the β-carbon atom (the one bonded to the $-CH_2S$ group). The tilt angle θ is then defined as the angle between the chain direction and the surface normal, as shown in Figure 1b. The tilt direction ϕ is the angle between the S−S NN direction and the projection of the chain direction onto the surface plane. The twist angle χ is given by the dihedral angle between the backbone plane (conveniently represented by the S−C—C plane, i.e., the one determined by sulfur, α-carbon and β-carbon atoms) and the plane determined by the chain direction and the surface normal.

2.2. Interaction Potential. For SAMs on metal surfaces, the molecule−substrate interaction may be important and cause the disordering of interfacial metal atoms. For instance, GIXD experiments and DFT simulations[59] have revealed that SAMs of hexanethiol on Au(111) can affect the sulfur−gold interface by a dynamical disorder with gold vacancies and addatoms partially distributed in the first layer. Nevertheless, it is also shown that the SAMs of hexanethiol still retain well-ordered hexagonal array despite the interfacial disordering.[59] Therefore, in the present work, no surface is explicitly considered in our MD simulations, since we aim at studying SAMs of alkylthiolates with chains containing at least three carbon atoms. That is to say, the only role of the surface in the simulation is to fix the sulfur headgroups at the positions of the adsorption sites corresponding to the hexagonal arrangement. Therefore, the total potential energy of the system is given by the sum of the interatomic interactions among alkylthiolates. As shown previously in ref 67, this is a reasonable approximation for the chain lengths considered in this work. The potential energy surface that describes the interaction between alkylthiolates has been taken from ref 60. This potential is written as a sum of pairwise potentials following Buckingham equation:[68]

$$E_{\text{pot}} = \sum_{i<j}^{N} \left[A_{ij} \exp(-B_{ij} r_{ij}) - \frac{C_{ij}}{r_{ij}^6} \right] \quad (1)$$

where N is the total number of atoms in the system and the sum is over all pairs of atoms i and j. r_{ij} is the distance between atoms i and j. A_{ij}, B_{ij}, and C_{ij} are fitting parameters that depend on the type of atom (sulfur, carbon, or hydrogen). In our previous work,[60] we have obtained the values of the A_{ij}, B_{ij}, and C_{ij} parameters by fitting the above analytical formula to results obtained from MP2 computations performed for alkylthiolates in the absence of the metal substrate.

2.3. Setup of MD Simulations. The MD simulations have been performed using the DL_POLY2 package.[69] We have treated each molecule as a rigid body; that is, the intramolecular distances between any two atoms remain constant. This rigid-body approximation has been justified by a few simulations taking into account bond bending and rotation (see section 4.1). The geometry of the molecules is fully optimized by DFT calculations with the exchange-correlation functional of Perdew, Burke, and Ernzerhof (PBE)[70] using the VASP package.[71−73] All sulfur atoms are placed at fixed positions corresponding to the adsorption sites dictated by the hexagonal ordering (see Figure 1). By assigning infinite mass to sulfur atoms, their positions are unmovable during the whole simulation time. Each molecule is allowed to swing, rotate and twist by varying θ, ϕ, and χ angles, respectively.

The SAM is modeled using a 20 × 20 supercell containing 400 molecules, located throughout the surface plane by applying periodic boundary conditions. We have also tried other supercell models and confirmed that the 20 × 20 supercell has safely reached convergence for both energy and average tilt angle (see Figure S1 in Supporting Information).

A series of MD simulations with five different temperatures in descending order, T = 300, 200, 100, 50, and 10 K, are sequentially performed in canonical ensemble (NVT). At the beginning of the simulation for each temperature, Maxwell−Boltzmann distributed velocities are randomly assigned to all the atoms. The first simulation runs at 300 K for 500 ps with a time step of 0.5 fs. The simulation time and time step have been tested to be sufficiently large and small, respectively, to allow the system to evolve and reach thermodynamic equilibrium state. The first initial configuration is determined by a full potential energy surface (PES) scanning based on the single-chain model (see Section 4.2). That is to say, using a periodic unit cell containing a single molecule, the three-dimensional PES is generated as a function of θ, ϕ and χ angles. Then the structural configuration corresponding to the global minimum on the PES is taken as the initial configuration for the MD simulation on the unit cell containing 400 molecules. The first MD simulation is carried out at 300 K for 500 ps. The statistics are collected during the last 200 ps for the averages of energies and structural variables. The following MD simulation at the next lower temperature is performed during 200 ps, starting from the configuration obtained in the previous MD simulation performed at higher temperature. The statistical information is collected over the last 100 ps for these simulations at lower temperatures. The same procedure is used for MD simulations at lower temperatures.

In addition, a few annealing simulations have been carried out which validate the MD simulations described above (see Supporting Information). We also compared MD simulations with MC simulations for C_6 and C_{10} on Au(111) and Ag(111) surfaces. Both MD and MC results are in reasonable agreement with each other (see Supporting Information).

3. RESULTS

3.1. C_n on Au(111). The MD-simulated average tilt angles $\langle\theta\rangle$ of thiolates C_n on Au(111) are summarized in Figure 2 and compared with various available experimental measurements. As we can see, our theoretical tilt angles at 300 K (solid line with empty circles) are in good agreement with most of the experimental measurements at room temperature (full symbols). In order to compare experiment[28] at 4 K, the theoretical results simulated at 10 K are also presented by dashed line in Figure 2. Still, the comparison shows a satisfying agreement. These results validate the assumed theoretical conditions used in our MD simulations, indicating that the dominant factor of molecular orientations of alkylthiolate chains on Au(111) is mainly intermolecular vdW interactions. The tilt angles at room temperature obtained in previous theoretical work[53,54,56,58] are also given in Figure 2. Among these theoretical works, only that of ref 56 has performed a systematic MD study of the variation of the tilt angle with chain length by using a UA FF. As can been in Figure 2, the overall agreement with the available experimental data is better for our data. The other theoretical results[53,54,58] presented in Figure 2 have reported tilt angles only for a few chain lengths (typically

dx.doi.org/10.1021/jp412285v | J. Phys. Chem. A XXXX, XXX, XXX−XXX

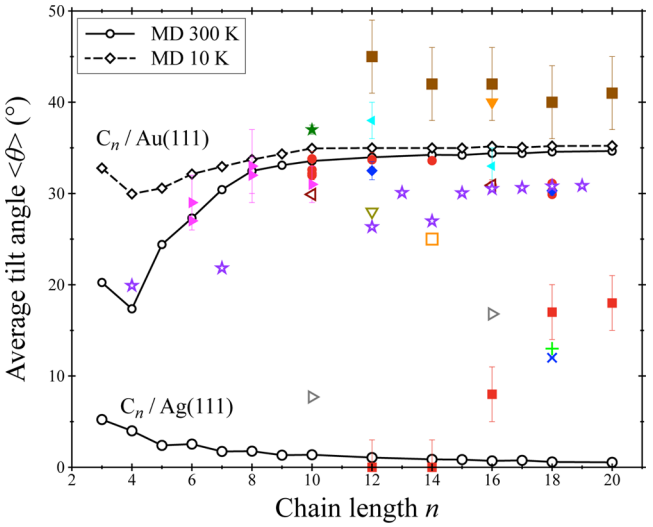

Figure 2. Average tilt angle $\langle\theta\rangle$ as a function of chain length n obtained from the MD simulations (empty symbols) in the present and the previous work and from the experiments (filled symbols). Solid and dashed lines indicate simulation results at 300 and 10 K, respectively. Filled circles,[21] filled diamonds,[14] filled five-pointed star,[20] filled brown squares,[27] filled down-pointing triangles[22] and filled left-pointing triangles[26] correspond to experiments on Au(111) at room temperature, and filled right-pointing triangles[28] indicate experiments on Au(111) at 4 K. Filled red squares,[27] filled cross[74] and x mark[24] correspond to experiments on Ag(111) around room temperature. Empty five-pointed stars,[56] empty square,[58] empty down-pointing triangle,[53] and empty left-pointing triangles[54] represent the simulated tilt angles on Au(111) at room temperature by other theoretical work. Empty right-pointing triangles[54] show the simulated tilt angles on Ag(111) at room temperature by other work.

one or two in the range of chain lengths considered in the present work).

In addition, as shown by Figure 2, the average tilt angle $\langle\theta\rangle$ of C_n ($n \geqslant 4$) on Au(111) slightly increases as the chain length n increases and reaches an almost constant value of ~35° for $n \geqslant 10$.

In order to investigate the effect of temperature on the structures of C_n SAMs, simulated results at 300, 200, 100, 50, and 10 K are compared in Figure 3. In Figure 3 (a), we can see that as the temperature increases the average tilt angle $\langle\theta\rangle$ decreases in all the cases of C_n on Au(111). But the effect of temperature is becoming less important as the chain length increases. For instance, when the system cools from 300 to 10 K, $\langle\theta\rangle$ increases significantly from 17° to 30° for C_4, while the increase of $\langle\theta\rangle$ is within 2° for longer chains C_n ($n \geqslant 10$).

Figure 4 shows the distributions of the three angles for C_4, C_{10}, and C_{16} on Au(111) at different temperatures. As expected,

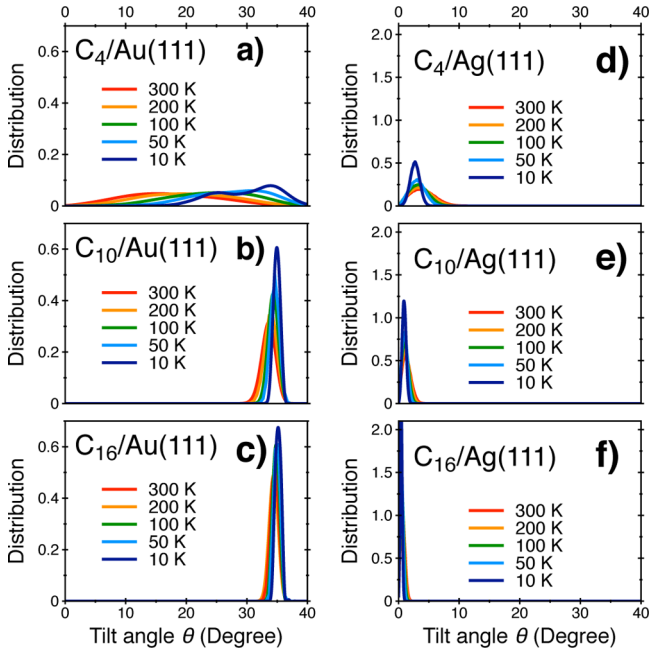

Figure 4. Distribution of tilt angle for C_4, C_{10} and C_{16} on Au(111) and Ag(111).

the distributions of these angles become narrower and sharper as temperature decreases since the decreasing thermal energy leads to less population on higher energy states in the system. Moreover, at the same temperature, longer chains reveal narrower distribution of tilt angle than shorter chains.

3.2. C_n on Ag(111). The simulated average tilt angles $\langle\theta\rangle$ of C_n on Ag(111) surface are within 5°, much smaller than those on the Au(111) surface, as we can see in Figure 2. This is in agreement with experimental measurements for C_{12} and C_{14} on Ag(111).[27] However, there is a remarkable disagreement between theoretical and experimental tilt angles for C_n beyond C_{16} (see Figure 2). For example, the simulated tilt angle of C_{18} on Ag(111) is only 0.6°, while the experimental estimation is

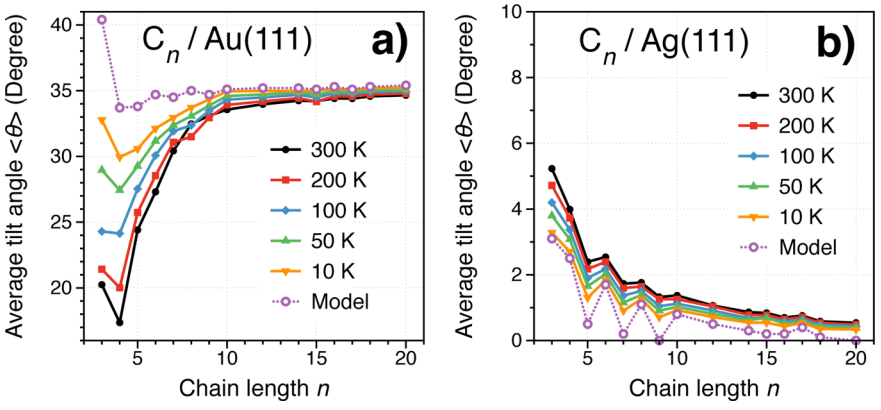

Figure 3. Average tilt angle $\langle\theta\rangle$ as a function of chain length n, obtained from simulations at different temperatures for C_n on Au(111) and Ag(111). Dotted line with empty circles shows the optimal angle corresponding to the lowest energy configuration using the single-chain model of C_n SAMs.

dx.doi.org/10.1021/jp412285v | J. Phys. Chem. A XXXX, XXX, XXX−XXX

Table 1. Average Tilt Angles (in deg.) Obtained from MD Simulations without and with the Inclusion of Bond Bending and Rotation[a]

		C_{10}		C_{14}		C_{16}	
surface	temp (K)	rigid	flexible	rigid	flexible	rigid	flexible
Au(111)	300	$33.6_{\pm 1.1}$	$(24.2_{\pm 5.7})$	$30.1_{\pm 1.9}$	$(25.5_{\pm 5.5})$	$31.1_{\pm 1.6}$	$(27.0_{\pm 5.6})$
	10	$34.9_{\pm 0.4}$	$(35.1_{\pm 0.8})$	$33.9_{\pm 2.1}$	$(34.2_{\pm 0.7})$	$33.9_{\pm 1.7}$	$(36.2_{\pm 0.7})$
Ag(111)	300	$1.4_{\pm 0.7}$	$(4.9_{\pm 2.7})$	$0.9_{\pm 0.4}$	$(5.1_{\pm 2.6})$	$0.7_{\pm 0.4}$	$(5.0_{\pm 2.3})$
	10	$0.9_{\pm 0.3}$	$(3.0_{\pm 0.9})$	$0.5_{\pm 0.2}$	$(2.4_{\pm 0.6})$	$0.4_{\pm 0.2}$	$(3.1_{\pm 0.6})$

[a]The values inside parentheses are results using flexible molecular chains, and the values outside of parentheses are results using rigid molecular chains. Subscript numbers indicate standard deviations.

about 17°[27] or 12°−13°.[24,75] Monte Carlo simulations carried out in previous work[54] predict a tilt angle of 17° for C_{16} on Ag(111), which is larger than the experimental value. Therefore, in view that available experimental measurements for C_n SAMs Ag(111) are rather scarce, more experiments would be necessary in order to clarify this issue.

As pointed out by Vemparala and co-workers,[58] the difference of tilt angle between C_n SAMs on Au(111) and those on Ag(111) can be qualitatively understood based on a simple picture as follows. Assuming that the vdW interaction among upright chains as a function of interchain spacing has a minimum at a_{min} = 4.7 Å, for a given interchain spacing $a > a_{min}$ the vdW attraction is to be maximized by tilting the chains by a certain angle $\theta = \cos^{-1}(3/[4(a/a_{min})^2 - 1])^{1/2}$. This gives an estimated tilt angle of 23° for C_n on Au(111).[58] In the case of Ag(111), the chains keep upright since the interchain vdW interaction is always repulsive ($a < a_{min}$).

Contrary to the case of Au(111) substrate, for C_n on Ag(111), when the chain length increases the average tilt angle decreases, as demonstrated in Figure 4d. It is also interesting to see that the average tilt angle increases as temperature increases, showing the opposite effect to that in the case of C_n on Au(111). To understand these differences, a simple model is proposed and discussed in the next section.

One may notice an odd−even effect in the variation of tilt angle with chain length for C_n on Ag(111), as shown in Figure 3b. This is probably due to the alternation of bond lengths in the C_n alkylthiolates. According to our DFT geometry optimization for the C_n (n = 1−6) molecules, the C−C bond lengths show short−long−short alternation, which could be responsible for the odd−even effect observed in Figure 3b. Nevertheless, this effect is rather small (∼1°) and vanishes for longer chains and at higher temperatures.

4. DISCUSSION

4.1. Effect of Bond Bending and Rotation. The MD results presented in the previous section were obtained by treating the whole alkylthiolate molecule as a rigid body. In order to reveal the importance of the inclusion of bond bending and rotation, we have performed several MD simulations allowing all the S−C and C−C bonds to bend and rotate.

The bond bending interactions are described by a harmonic valence angle potential

$$U_{bend}(\alpha) = \frac{k_b}{2}(\alpha - \alpha_0)^2$$

where α is the bond angle, α_0 the optimal bond angle and k_b the force constant. The recommended values[54] of parameters α_0 and k_b are α_0 = 114.4°, k_b = 5.386 eV rad^{-2} for S−C—C bond angle and α_0 = 109.5°, k_b = 5.386 eV rad^{-2} for C−C—C bond angle, respectively.

The bond rotation interactions are included using the Ryckaert-Bellemans dihedral angle potential[54,76]

$$U_{rot}(\psi) = \sum_{i=0}^{5} a_i \cos^i(\psi)$$

where ψ is the dihedral angle of S−C—C−C or C−C—C−C bonds, and the empirical parameters a_i are +0.09614, +0.1260, −0.1359, −0.03170, 0.2719, and −0.3264 eV for i = 0−5, respectively.

The average tilt angles obtained from MD simulations without and with the inclusion of bond bending and rotation are compared in Table 1 for some systems. As we can see from Table 1, the inclusion of bond bending and rotation in the simulations does not change very much the values of the average tilt angle, compared to the rigid-body approximation. In this work, we have defined the tilt angle as the angle between the surface normal and the line connecting the sulfur atom and the beta-carbon atom (i.e., the second atom next to sulfur). The latter coincides with the average chain direction in the rigid model, but differs from it in the flexible chain model, since the bonds are allowed to bend, swing and rotate. This gives rise to some apparent deviations in tilt angle, especially at higher temperatures. In any case, notice that, at the lowest temperature considered in Table 1, the difference between rigid- and flexible-chain models is very small (1−2 degrees). At higher temperature, the differences seem to be larger, but standard deviations in the flexible-chain results are also much larger (partly due to our definition of the tilt angle and not to a really physical effect), such that there is not a real incompatibility between rigid- and flexible-chain results. The largest deviation is found for C_{10} on Au(111) at 300 K, for which the difference is about 9.4°. However, all the other cases listed in Table 1 show fairly good agreement (within 5°) between the rigid-body and the flexible molecular models. Additionally, we can also see that the inclusion of bond bending and rotation slightly broadens the distribution of tilt angles, which is due to the increase of degrees of freedom considered in the more flexible model.

4.2. Interpretation by the Single-Chain Model. As we have seen in Section 3, SAMs of alkylthiolate on Au(111) and Ag(111) surfaces have quite different molecular orientations and the temperature and chain length dependences of tilt angle are opposite between these two substrates. In order to understand these interesting behaviors, here we have proposed a simple model for alkylthiolate SAMs.

In this model, the SAM is represented by a periodically repeated unit cell containing only a single C_n molecule. Thus, in this model (hereafter referred to as "single-chain model") all molecules are equivalently oriented and the whole SAM is

dx.doi.org/10.1021/jp412285v | J. Phys. Chem. A XXXX, XXX, XXX−XXX

characterized by only three angles θ, ϕ and χ (see Figure 5). The minima of the three-dimensional potential energy surface

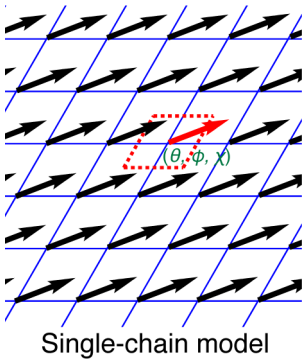

Figure 5. Schematic illustration of the single-chain model for the SAM of alkylthiolates on the (111) surface. The projection of molecules onto the surface plane is represented by black sticks, showing the tilt direction ϕ. Blue grids draw the lattice structure of the surface. Red dotted lines illustrate the unit cell in which the single molecular chain is highlighted in red.

$U(\theta,\phi,\chi)$ can be then easily determined. A one-dimensional potential energy $U(\theta,\phi_0,\chi_0)$ can be defined as a function of tilt angle θ, such that at a given value of θ the potential energy U takes the minimum value with ϕ_0 and χ_0 being the optimal tilt direction and the optimal twist angle, respectively. According to this definition, $U(\theta,\phi_0,\chi_0)$ can be regarded as the minimum potential energy path when varying tilt angle θ along the potential energy surface.

It is worth mentioning that, for long-chain C_n ($n \geqslant 10$) on both Au(111) and Ag(111) at 10 K, the values of θ_0, ϕ_0, and χ_0 for the global minimum in the single-chain model are in good agreement with the average values obtained from the MD calculations (see Figure 3). This agreement implies that in our MD simulated systems cooled from room temperature down to 10 K, the structure of the SAM would be close to global minimum configuration. It also indicates that the single-chain model is a reasonable simplification for the SAM of long-chain alkylthiolates C_n ($n \geqslant 10$).

Then, the effect of temperature can be understood by using the single-chain model of the SAM of alkylthiolates. As mentioned in section 3, the average tilt angle of C_n on Au(111) decreases as temperature increases. Let us take a look at the $U(\theta,\phi_0,\chi_0)$ curve for C_4 on Au(111) in Figure 6a. At a certain temperature T, as we can see in Figure 6a, higher energy states are populated due to thermal excitation within an energy window kT (being k the Boltzmann constant), leading to a significant spread of tilt angle θ around θ_0, the tilt angle corresponding to the global minimum. We can see in Figure 6a that the interval of accessible θ values is not symmetric around θ_0; there are significantly more energetically accessible θ values below θ_0 than above θ_0, i.e., $\Delta\theta_- > \Delta\theta_+$. As a result, by averaging over the energy states within the expansion window, the mean tilt angle $\langle\theta\rangle$ becomes smaller and smaller as temperature T increases. Furthermore, as shown in Figure 6a, the $U(\theta,\phi_0,\chi_0)$ curves for C_{10} and C_{16} are much sharper than that for C_4, which explains the smaller effect of temperature on θ for longer chain alkylthiolates.

As we have seen, the temperature effect for C_n on Ag(111) is opposite to that on Au(111); the average tilt angle increases as temperature increases. This can also be understood in a similar

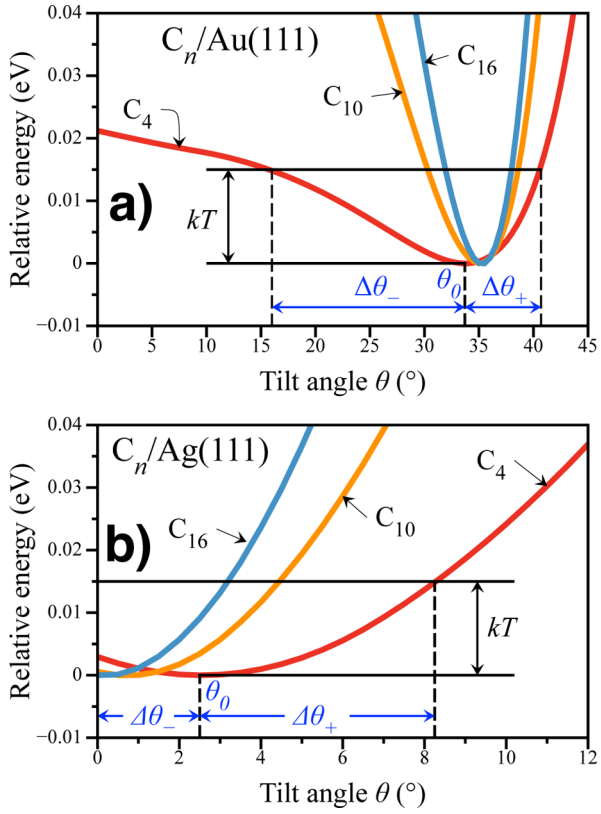

Figure 6. Lowest potential energy curves as functions of tilt angle θ for C_4, C_{10}, and C_{16} on (a) Au(111) and (b) Ag(111) based on the single-chain model. The energy zero is set to be the lowest energy corresponding to the global minimum on the PES for each chain length. The thermal energy at temperature T is indicated by an energy window kT, where k is Boltzmann constant. The corresponding spread of tilt angle θ due to thermal excitation is indicated by expansions $\Delta\theta_-$ and $\Delta\theta_+$ around θ_0 that corresponds to the global minimum.

way to that for Au(111) by looking at the potential energy curve as a function of θ based on the single-chain model. As can be seen (see Figure 3d), there is a fairly good agreement between the average tilt angle from the MD simulation at 10 K and the optimal tilt angle corresponding to the lowest energy configuration based on the single-chain model. Figure 6b illustrates the thermal spread of the tilt angle for C_4 on Ag(111) at a certain temperature T. It is clear that the interval of accessible θ values above θ_0, $\Delta\theta_+$, is larger than that below θ_0, $\Delta\theta_-$. As a result, the average tilt angle within the thermally spread window increases as temperature T increases.

In addition, at the same temperature, longer chains reveal narrower distribution of tilt angle than shorter ones, as demonstrated in Figure 4. This is due to the fact that the former gives sharper $U(\theta,\phi_0,\chi_0)$ curves than the latter (see Figure 6). It is also worth mentioning that the discussion based on the single-chain model can be made quantitative by applying principles of statistical mechanics. By averaging over the Boltzmann distribution of tilt angles along the potential energy curve in Figure 6, we have calculated the tilt angles of C_{10} and C_{16} on Au(111) and Ag(111) at various temperatures. The results for the tilt angle and temperature dependences are in good agreement with those obtained from the MD simulations (see the Supporting Information).

dx.doi.org/10.1021/jp412285v | J. Phys. Chem. A XXXX, XXX, XXX−XXX

5. CONCLUSIONS

In conclusion, we have presented a systematic MD study of the structure of hexagonally packed SAMs of alkylthiolates on various metal surfaces, with especial attention to Au(111) and Ag(111). The MD simulations have been performed by using a recently developed FF based on MP2 calculations. Good agreement between the present results and the existing experimental data is found for Au(111). Variations in the structure of these SAMs as a function of temperature, alkyl-chain length, and anchorage-site spacing have been investigated. We have found that, on Au(111), the average tilt angle slightly increases with chain length up to around 30°, while it slightly decreases on Ag(111) from around 5° down to almost 0°. For both systems, the variation with temperature is small and is the opposite for Au(111) and Ag(111). The present results also show that the key parameter that makes the geometry of SAMs so different on Au(111) and Ag(111) is the anchorage-site spacing. All the results can be easily understood by means of a simple single-chain model. The predictions of the MD calculations are confirmed by representative Monte Carlo simulations performed with the same FF.

■ ASSOCIATED CONTENT

Ⓢ Supporting Information

The convergence test for the size of supercell; details for the annealing simulations and MC simulations; quantitative results based on the single-chain model; the complete author list of ref 66. This material is available free of charge via the Internet at http://pubs.acs.org.

■ AUTHOR INFORMATION

Corresponding Author

*E-mail: yang.wang@uam.es. Phone: +34 914972573. Fax: +34 914975238.

Notes

The authors declare no competing financial interest.

■ ACKNOWLEDGMENTS

We thank the CCC-UAM and the RES for allocation of computer time. Work was partially supported by the projects FIS2010-15127, CTQ2010-17006, and CSD2007-00010 (MICINN, Spain); S2009/MAT1726 (CAM, Spain); A2/039631/11 (AECID, Spain); PIP 0667 (CONICET, Argentina); and PICT Bicentenario 1962 (ANPCyT, Argentina).

■ REFERENCES

(1) Ulman, A. Formation and Structure of Self-Assembled Monolayers. *Chem. Rev.* **1996**, *96*, 1533−1554.

(2) Schreiber, F. Self-assembled monolayers: from 'simple' model systems to biofunctionalized interfaces. *J. Phys.: Condens. Matter* **2004**, *16*, R881−R900.

(3) Love, J. C.; Estroff, L. A.; Kriebel, J. K.; Nuzzo, R. G.; Whitesides, G. M. Self-Assembled Monolayers of Thiolates on Metals as a Form of Nanotechnology. *Chem. Rev.* **2005**, *105*, 1103−1170.

(4) Dubois, L.; Zegarski, B.; Nuzzo, R. Molecular ordering of organosulfur compounds on Au(111) and Au(100): Adsorption from solution and in ultrahigh vacuum. *J. Chem. Phys.* **1993**, *98*, 678−688.

(5) Schreiber, F. Structure and growth of self-assembling monolayers. *Prog. Surf. Sci.* **2000**, *65*, 151−257.

(6) Vericat, C.; Vela, M. E.; Salvarezza, R. C. Self-assembled monolayers of alkanethiols on Au(111): surface structures, defects and dynamics. *Phys. Chem. Chem. Phys.* **2005**, *7*, 3258−3268.

(7) Nuzzo, R. G.; Allara, D. L. Adsorption of bifunctional organic disulfides on gold surfaces. *J. Am. Chem. Soc.* **1983**, *105*, 4481−4483.

(8) Chidsey, C. E.; Loiacono, D. N. Chemical functionality in self-assembled monolayers: structural and electrochemical properties. *Langmuir* **1990**, *6*, 682−691.

(9) Strong, L. Structures of self-assembled monolayer films of organosulfur compounds adsorbed on gold single crystals: electron diffraction studies. *Langmuir* **1988**, *4*, 546−558.

(10) Camillone, N.; Chidsey, C. E. D.; Liu, G.; Scoles, G. Superlattice structure at the surface of a monolayer of octadecanethiol self-assembled on Au(111). *J. Chem. Phys.* **1993**, *98*, 3503−3511.

(11) Camillone, N.; Chidsey, C. E. D.; Liu, G.; Scoles, G. Substrate dependence of the surface structure and chain packing of docosyl mercaptan self-assembled on the (111), (110), and (100) faces of single crystal gold. *J. Chem. Phys.* **1993**, *98*, 4234−4245.

(12) Camillone, N.; Chidsey, C. E. D.; Eisenberger, P.; Fenter, P.; Li, J.; Liang, K. S.; Liu, G.; Scoles, G. Structural defects in self-assembled organic monolayers via combined atomic beam and X-ray diffraction. *J. Chem. Phys.* **1993**, *99*, 744−747.

(13) Stettner, J.; Winkler, A. Characterization of Alkanethiol Self-Assembled Monolayers on Gold by Thermal Desorption Spectroscopy. *Langmuir* **2010**, *26*, 9659−9665.

(14) Fenter, P.; Eisenberger, P.; Liang, K. S. Chain-length dependence of the structures and phases of $CH_3(CH_2)_{n-1}$ SH self-assembled on Au(111). *Phys. Rev. Lett.* **1993**, *70*, 2447−2450.

(15) Barrena, E.; Ocal, C.; Salmeron, M. Evolution of the structure and mechanical stability of self-assembled alkanethiol islands on Au(111) due to diffusion and ripening. *J. Chem. Phys.* **1999**, *111*, 9797−9802.

(16) Poirier, G. E.; Tarlov, M. J. The c(4 × 2) Superlattice of n-Alkanethiol Monolayers Self-Assembled on Au(111). *Langmuir* **1994**, *10*, 2853−2856.

(17) Delamarche, E.; Michel, B.; Gerber, C.; Anselmetti, D.; Guentherodt, H.-J.; Wolf, H.; Ringsdorf, H. Real-Space Observation of Nanoscale Molecular Domains in Self-Assembled Monolayers. *Langmuir* **1994**, *10*, 2869−2871.

(18) Bucher, J. P.; Santesson, L.; Kern, K. Selective imaging of self-assembled monolayers by tunneling microscopy. *Appl. Phys. A: Mater. Sci.* **1994**, *59*, 135−138.

(19) Anselmetti, D.; Baratoff, A.; Güntherodt, H.-J.; Delamarche, E.; Michel, B.; Kang, C. G. H.; Wolf, H.; Ringsdorf, H. Domain and Molecular Superlattice Structure of Dodecanethiol Self-Assembled on Au(111). *Europhys. Lett.* **1994**, *27*, 365−370.

(20) Fenter, P.; Eberhardt, A.; Eisenberger, P. Self-Assembly of *n*-Alkyl Thiols as Disulfides on Au(111). *Science* **1994**, *266*, 1216−1218.

(21) Fenter, P.; Eberhardt, A.; Liang, K. S.; Eisenberger, P. Epitaxy and chainlength dependent strain in self-assembled monolayers. *J. Chem. Phys.* **1997**, *106*, 1600−1608.

(22) Nuzzo, R.; Dubois, L.; Allara, D. Fundamental studies of microscopic wetting on organic surfaces. 1. Formation and structural characterization of a self-consistent series of polyfunctional organic monolayers. *J. Am. Chem. Soc.* **1990**, *112*, 558−569.

(23) Nuzzo, R. G.; Korenic, E. M.; Dubois, L. H. Studies of the temperature-dependent phase behavior of long chain n-alkyl thiol monolayers on gold. *J. Chem. Phys.* **1990**, *93*, 767−773.

(24) Laibinis, P. E.; Whitesides, G. M.; Allara, D. L.; Tao, Y.-T.; Parikh, A. N.; Nuzzo, R. G. Comparison of the structures and wetting properties of self-assembled monolayers of n-alkanethiols on the coinage metal surfaces, copper, silver, and gold. *J. Am. Chem. Soc.* **1991**, *113*, 7152−7167.

(25) Hähner, G.; Kinzler, M.; Thümmler, C.; Wöll, C.; Grunze, M. Structure of self-organizing organic films: A near edge x-ray absorption fine structure investigation of thiol layers adsorbed on gold. *J. Vac. Sci. Technol. A* **1992**, *10*, 2758−2763.

(26) Fischer, D.; Marti, A.; Hähner, G. Obtaining a physical two-dimensional Cartesian reference. *J. Vac. Sci. Technol. A* **1997**, *15*, 2173−2176.

(27) Ehler, T. T.; Malmberg, N.; Noe, L. J. Characterization of Self-Assembled Alkanethiol Monolayers on Silver and Gold Using Surface Plasmon Spectroscopy. *J. Phys. Chem. B* **1997**, *101*, 1268−1272.
(28) Han, P.; Kurlanda, A. R.; Giordano, A. N.; Nanayakkara, S. U.; Blake, M. M.; Pochas, C. M.; Weiss, P. S. Heads and Tails: Simultaneous Exposed and Buried Interface Imaging of Monolayers. *ACS Nano* **2009**, *3*, 3115−3121.
(29) Abufager, P.; Soria, L. A.; Martiarena, M.; Reuter, K.; Busnengo, H. Structure of the methylthiolate monolayer on Ag (111): The role of substrate vacancies. *Chem. Phys. Lett.* **2011**, *503*, 71−74.
(30) Harris, A. L.; Chidsey, C. E. D.; Levinos, N. J.; Loiacono, D. N. Monolayer vibrational spectroscopy by infrared-visible sum generation at metal and semiconductor surfaces. *Chem. Phys. Lett.* **1987**, *141*, 350−356.
(31) Harris, A. L.; Rthberg, L.; Dubois, L. H.; Levinos, N. J.; Dhar, L. Molecular vibrational energy relaxation at a metal surface: Methyl thiolate on Ag(111). *Phys. Rev. Lett.* **1990**, *64*, 2086−2089.
(32) Harris, A. L.; Rothberg, L.; Dhar, L.; Levinos, N. J.; Dubois, L. H. Vibrational energy relaxation of a polyatomic adsorbate on a metal surface: Methyl thiolate (CH_3S) on Ag(111). *J. Chem. Phys.* **1991**, *94*, 2438−2448.
(33) Abufager, P.; Solano Canchaya, J.; Wang, Y.; Alcami, M.; Martin, F.; Soria, L. A.; Martiarena, M.; Reuter, K.; Busnengo, H. Theoretical study of the structure of self-assembled monolayers of short alkylthiolates on Au(111) and Ag(111): the role of induced substrate reconstruction and chain-chain interactions. *Phys. Chem. Chem. Phys.* **2011**, *13*, 9353−9362.
(34) Bosio, S. B. M.; Hase, W. L. Energy transfer in rare gas collisions with self-assembled monolayers. *J. Chem. Phys.* **1997**, *107*, 9677−9686.
(35) Yan, T.; Hase, W. L. Origin of the Boltzmann translational energy distribution in the scattering of hyperthermal Ne atoms off a self-assembled monolayer. *Phys. Chem. Chem. Phys.* **2000**, *2*, 901−910.
(36) Yan, T.; Hase, W. L.; Barker, J. R. Identifying trapping desorption in gas−surface scattering. *Chem. Phys. Lett.* **2000**, *329*, 84−91.
(37) Yan, T.; Hase, W. L. Comparisons of Models for Simulating Energy Transfer in Ne-Atom Collisions with an Alkyl Thiolate Self-Assembled Monolayer. *J. Phys. Chem. B* **2002**, *106*, 8029−8037.
(38) Yan, T.; Isa, N.; Gibson, K. D.; Sibener, S. J.; Hase, W. L. Role of Surface Intramolecular Dynamics in the Efficiency of Energy Transfer in Ne Atom Collisions with a n-Hexylthiolate Self-Assembled Monolayer. *J. Phys. Chem. A* **2003**, *107*, 10600−10607.
(39) Isa, N.; Gibson, K. D.; Yan, T.; Hase, W.; Sibener, S. J. Experimental and simulation study of neon collision dynamics with a 1-decanethiol monolayer. *J. Chem. Phys.* **2004**, *120*, 2417−2433.
(40) Tasić, U. S.; Yan, T.; Hase, W. L. Dynamics of Energy Transfer in Collisions of $O(^3P)$ Atoms with a 1-Decanethiol Self-Assembled Monolayer Surface. *J. Phys. Chem. B* **2006**, *110*, 11863−11877.
(41) Schultz, D. G.; Wainhaus, S. B.; Hanley, L.; de Sainte Claire, P.; Hase, W. L. Classical dynamics simulations of $SiMe_3^+$ ion-surface scattering. *J. Chem. Phys.* **1997**, *106*, 10337−10348.
(42) Bosio, S. B.; Hase, W. L. Simulations of energy transfer in Cr(CO)6+ surface-induced dissociation. *Int. J. Mass Spectrom. Ion Processes* **1998**, *174*, 1−9.
(43) Meroueh, O.; Hase, W. L. Effect of surface stiffness on the efficiency of surface-induced dissociation. *Phys. Chem. Chem. Phys.* **2001**, *3*, 2306−2314.
(44) Meroueh, O.; Hase, W. L. Dynamics of Energy Transfer in PeptideâĹŠSurface Collisions. *J. Am. Chem. Soc.* **2002**, *124*, 1524−1531.
(45) Barnes, G. L.; Hase, W. L. Energy Transfer, Unfolding, and Fragmentation Dynamics in Collisions of N-Protonated Octaglycine with an H-SAM Surface. *J. Am. Chem. Soc.* **2009**, *131*, 17185−17193.
(46) Hautman, J.; Klein, M. L. Simulation of a monolayer of alkyl thiol chains. *J. Chem. Phys.* **1989**, *91*, 4994−5001.
(47) Hautman, J.; Klein, M. L. Molecular dynamics simulation of the effects of temperature on a dense monolayer of long-chain molecules. *J. Chem. Phys.* **1990**, *93*, 7483−7492.
(48) Siepmann, J. I.; McDonald, I. R. Domain formation and system-size dependence in simulations of self-assembled monolayers. *Langmuir* **1993**, *9*, 2351−2355.
(49) Tupper, K. J.; Colton, R. J.; Brenner, D. W. Simulations of Self-Assembled Monolayers under Compression: Effect of Surface Asperities. *Langmuir* **1994**, *10*, 2041−2043.
(50) Pertsin, A. J.; Grunze, M. Low-Energy Structures of a Monolayer of Octadecanethiol Self-Assembled on Au(111). *Langmuir* **1994**, *10*, 3668−3674.
(51) Bhatia, R.; Garrison, B. J. Phase Transitions in a Methyl-Terminated Monolayer Self-Assembled on Au111. *Langmuir* **1997**, *13*, 765−769.
(52) Bhatia, R.; Garrison, B. J. Structure of c(4 × 2) Superlattice in Alkanethiolate Self-Assembled Monolayers. *Langmuir* **1997**, *13*, 4038−4043.
(53) Zhang, L.; Goddard, W. A.; Jiang, S. Molecular simulation study of the c(4 × 2) superlattice structure of alkanethiol self-assembled monolayers on Au(111). *J. Chem. Phys.* **2002**, *117*, 7342−7349.
(54) Alexiadis, O.; Harmandaris, V. A.; Marvrantzas, V. G.; Site, L. D. Atomistic Simulation of Alkanethiol Self-Assembled Monolayers on Different Metal Surfaces via a Quantum, First-Principles Parametrization of the Sulfur-Metal Interaction. *J. Phys. Chem. C* **2007**, *111*, 6380−6391.
(55) Alexiadis, O.; Daoulas, K. C.; Marvrantzas, V. G. An Efficient Monte Carlo Algorithm for the Fast Equilibration and Atomistic Simulation of Alkanethiol Self-Assembled Monolayers on a Au(111) Substrate. *J. Phys. Chem. B* **2008**, *112*, 1198−1211.
(56) Ramin, L.; Jabbarzadeh, A. Odd-Even Effects on the Structure, Stability, and Phase Transition of Alkanethiol Self-Assembled Monolayers. *Langmuir* **2011**, *27*, 9748−9759.
(57) Rai, B.; P, S.; Malhotra, C. P.; Pradip; Ayappa, K. G. Molecular Dynamic Simulations of Self-Assembled Alkylthiolate Monolayers on an Au(111) Surface. *Langmuir* **2004**, *20*, 3138−3144.
(58) Vemparala, S.; Karki, B. B.; Kalia, R. K.; Nakano, A.; Vashishta, P. Large-scale molecular dynamics simulations of alkanethiol self-assembled monolayers. *J. Chem. Phys.* **2004**, *121*, 4323−4330.
(59) Cossaro, A.; Mazzarello, R.; Rousseau, R.; Casalis, L.; Verdini, A.; Kohlmeyer, A.; Floreano, L.; Scandolo, S.; Morgante, A.; Klein, M.; Scoles, G. X-ray diffraction and computation yield the structure of alkanethiols on gold(111). *Science* **2008**, *321*, 943−946.
(60) Solano Canchaya, J.; Wang, Y.; Alcamí, M.; Martín, F.; Busnengo, H. Study of the interaction between short alkanethiols from ab initio calculations. *Phys. Chem. Chem. Phys.* **2010**, *12*, 7555−7565.
(61) Torres, E.; Blumenau, A. T.; Biedermann, P. U. Steric and Chain Length Effects in the $(\sqrt{3}\times\sqrt{3})R30°$ Structures of Alkanethiol Self-Assembled Monolayers on Au(111). *ChemPhysChem* **2011**, *12*, 999−1009.
(62) Grimme, S. Accurate description of van der Waals complexes by density functional theory including empirical corrections. *J. Comput. Chem.* **2004**, *25*, 1463−1473.
(63) Grimme, S. Semiempirical GGA-type density functional constructed with a long-range dispersion correction. *J. Comput. Chem.* **2006**, *27*, 1787−1799.
(64) Mar, W.; Klein, M. L. Molecular dynamics study of the self-assembled monolayer composed of $S(CH_2)_{14}CH_3$ molecules using an all-atoms model. *Langmuir* **1994**, *10*, 188−196.
(65) Frederiksen, T.; Munuera, C.; Ocal, C.; Brandbyge, M.; Paulsson, M.; Sanchez-Portal, D.; Arnau, A. *ACS Nano* **2009**, *3*, 2073−2080.
(66) Shpaisman, H.; Seitz, O.; Yaffe, O.; Roodenko, K.; Scheres, L.; Zuilhof, H.; Chabal, Y. J.; Sueyoshi, T.; Kera, S.; Ueno, N.; et al. Structure Matters: Correlating temperature dependent electrical transport through alkyl monolayers with vibrational and photoelectron spectroscopies. *Chem. Sci.* **2012**, *3*, 851−862.
(67) Wang, Y.; Solano Canchaya, J. G.; Alcamí, M.; Busnengo, H. F.; Martín, F. *J. Am. Chem. Soc.* **2012**, *134*, 13224.
(68) Buckingham, R. A. The Classical Equation of State of Gaseous Helium, Neon and Argon. *Proc. R. Soc. London A* **1938**, *168*, 264−283.

(69) Smith, W.; Forester, T.; Todorov, I.; Leslie, M. *THE DL_POLY 2 USER MANUAL*; CCLRC Daresbury Laboratory: Daresbury, U.K., 2006.
(70) Perdew, J. P.; Burke, W.; Ernzerhof, M. Generalized Gradient Approximation Made Simple. *Phys. Rev. Lett.* **1996**, *77*, 3865−3868.
(71) Kresse, G.; Hafner, J. Ab initio molecular-dynamics simulation of the liquid-metal-amorphous-semiconductor transition in germanium. *Phys. Rev. B* **1994**, *49*, 14251−14269.
(72) Kresse, G.; Furthmüller, J. Efficient iterative schemes for ab initio total-energy calculations using a plane-wave basis set. *Phys. Rev. B* **1996**, *54*, 11169−11186.
(73) Kresse, G.; Furthmüller, J. Efficiency of ab-initio total energy calculations for metals and semiconductors using a plane-wave basis set. *Comput. Mater. Sci.* **1996**, *6*, 15−50.
(74) Walczak, M. M.; Chung, C.; Stole, S. M.; Widrig, C. A.; Porter, M. D. Structure and interfacial properties of spontaneously adsorbed n-alkanethiolate monolayers on evaporated silver surfaces. *J. Am. Chem. Soc.* **1991**, *113*, 2370−2378.
(75) Wahnström, G.; Lee, A. B.; Strömquist, J. Motion of "hot" oxygen adatoms on corrugated metal surfaces. *J. Chem. Phys.* **1996**, *105*, 326−336.
(76) Ryckaert, J. P.; Bellemans, A. Molecular dynamics of liquid n-butane near its boiling point. *Chem. Phys. Lett.* **1990**, *30*, 123−125.